High-Frequency Filtering Systems for Noise Measurements

Bachelor Thesis

Paul Ruhrberg

September 10, 2024

Group: Prof Dr. Erwann Bocquillon

Supervisor: Alina Rupp

Contents

1 Motivation

First experimentally observed in 2013, by the team led by Xue Qikun at Tsinghua University [1], the quantum anomalous Hall effect (QAHE) has recently attracted a lot of interest in the field of solid matter physics. In ferromagnetic materials, the transverse resistivity of the Hall effect has, in addition to the expected value, a term independent of the applied magnetic field. The term only depends on the material's magnetization and reaches a constant at saturation magnetization. This effect, known as the anomalous Hall effect, results from the combination of magnetic polarization and spin-orbit coupling. The QAHE is the quantized version of the anomalous hall effect. In quasi-2D magnetic topological isolators, the spontaneous magnetization of magnetic impurities breaks time-reversal symmetry and gives rise to a spinless chiral 1D edge state. Due to these edge states the resistance transverse to the direction of the current becomes quantized and the longitudinal resistance vanishes [2]. The realization of the spinless 1D chiral edge state leads to a good playground for 1D physics. The QAHE finds application in quantum computing and may lead to the development of low-power-consumption electronics [1]. Therefore the study of the different aspects and behaviors of these edge states is necessary.

The spinless 1D edge states can only be achieved at very low temperatures since the thermal energy can easily disrupt the stability of the material and ruin the quantized state. Therefore most measurements are done in a dilution refrigerator. This cryogenic device uses the phase transition of helium isotope mixture to cool down to a temperature on the order of 10 mK [3].

The longitudinal and transversal resistance can be measured through standard direct current (DC) equipment. Noise measurements can be used in addition to gain insight into the behavior of edge states, that can not be gained through the use of normal DC measurements. A current consists of the average current and fluctuations on top that are ever-present, known as noise. These fluctuations are caused by every component of the setup. In DC measurements noise is usually undesired and obstructs the desired data. However, in carefully constructed setups, the noise of the equipment can be reduced, leaving only the noise of the sample and the information it holds. The two types of noise commonly used for the

measurement of spinless 1D edge states are Johnson noise and shot noise. Johnson noise describes the random noise voltage created by thermal fluctuations of charge carriers. A resistor R without outside voltage applied generates a voltage across its length based on its temperature T

$$V_{noise} = \sqrt{4kTRB}. \tag{1}$$

k is the Boltzmann constant and B the band-width in hertz [4]. Shot noise compared to Johnson noise is only present when applying a voltage/current. In a simplified way charge carriers like electrons can be thought of as delivering a quantized charge amount in regular intervals to form a current. In reality, this regularity can be obstructed by different scattering processes, resulting in the fluctuation of the current. This so-called shot noise can only be present when the charge delivery is quantized and can therefore hold a lot of information on the scattering processes of conductors like the spinless 1D edge state [5]. Johnson noise and shot noise are classified as white noise because their amplitude is frequency-independent up to GHz. Together the measurement of Johnson noise and shot noise can give detailed information on heat transport and scattering of electrons in a sample [4].

To be able to measure noise at an effective level it is important to minimize the influence of disturbances on the signal. The biggest factors here are electromagnetic waves in the surroundings and the thermal noise created by the measurement equipment of the dilution refrigerator. A good improvement is achieved through the use of a filter system. A multitude of different filters that reduce disturbances at different frequencies as close to the sample as possible. The most common filter system consists of three different kinds of filters. A low-pass filter is used to filter at low frequencies, a π-filter (also called LC based on the used components) to filter intermediate frequencies, and metal powder filters to attenuate at high frequencies [6]. An infographic for the different frequency applications of these filters can be seen in figure 1.

Since the LC filter is too big to be included inside the dilution refrigerator, this thesis focuses only on the RC filter and the metal powder stage. The goal of this thesis is the design and

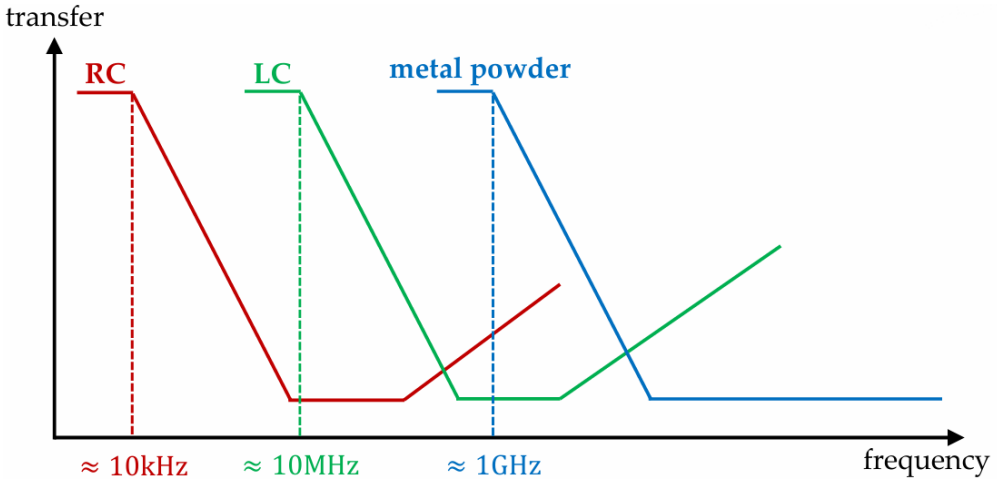

Figure 1: Filtering frequencies of three different filters. An RC filter, an LC filter, and a metal powder filter [6]

construction of a filter system that includes both an RC filter stage and a metal powder stage, to be used inside a dilution fridge for the optimization of noise measurements.

The thesis is separated into three main parts. The first chapter focuses on using electrical components to construct a circuit known as a low-pass filter. Therefore, basic electronics knowledge is reiterated, followed by the theory of low-pass filters, and concluded with the design and construction of such a circuit. The second chapter introduces the copper powder filter. A short introduction to the theory of metal powder filters is followed by the design and optimization process. The third chapter combines both filter stages and focuses on the application of such a filter at low temperatures. A conclusion and outlook is given at the end of this thesis.

2 RC-Filter Stage

The most basic of filtering systems can be achieved through fundamental electronic circuits. Depending on the desired filtering properties, these filters can be divided into low-pass, high-pass, or bandpass filters. As the name suggests a low-pass filter attenuates higher frequencies and lets lower frequencies pass. High-pass filters work the opposite way and attenuate the signal at low frequencies while allowing higher frequencies to pass. Band-pass filters differ by filtering out all frequencies except a certain "bandwidth" in which the frequencies are passed without attenuation. The band-stop filter works oppositely by letting all frequencies pass except a certain range where the signal is attenuated. The differences are visualized in figure 2. This chapter focuses on the low-pass variant, commonly known as an RC filter, (based on the components used) with the goal of attenuating frequencies in the higher kHz ranges while allowing the lower frequencies to pass through unfiltered. Electronic filters are made up of components known as resistors (R), capacitors (C) and inductors (L). The functionality of these components is the focus of the following chapter. The arising need for different types of filtering systems is a topic for chapters 3 and 4.

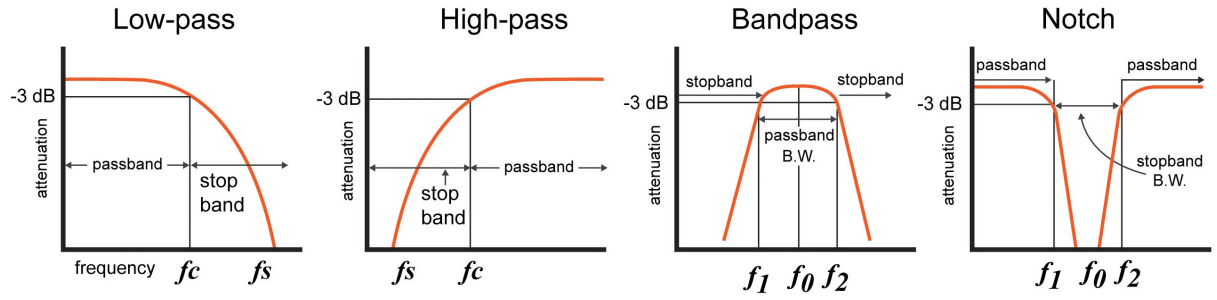

Figure 2: Visualization of different electronic filters and their pass-bands and stop-bands. Included are low-pass, high-pass, bandpass, and notch variants shown from left to right [7].

The underlying electronic principles will be reiterated in the following chapter to gain a thorough understanding of the functioning principles of RC filters.

2.1 Basics of Electronics

This first subsection will restate the basic concepts of alternating currents (AC). Afterwards, the components important for the discussion of electrical filters will be discussed.

2.1.1 Alternating Current

Time-dependent signals must be discussed first to understand the reaction of resistors, capacitors, and inductors in frequency-based filtering systems. In some cases, discussing voltage-current relations using imaginary numbers is advantageous. Since by definition no physical measurement yields imaginary quantities it is important to state that mathematical results will be interpreted for real values.

The most basic form of time-dependent voltage source is the sinusoidal source (AC voltage). The applied voltage $V(t)$ varies as a complex sinus function with the time t, described by the angular frequency $\omega = 2\pi f$, the amplitude V_0, and the phase shift ϕ.

$$V(t) = V_0 \cdot e^{i(\omega t + \phi)} \qquad \underline{V}(\omega') = V_0\sqrt{2\pi}\,\delta(\omega - \omega')\,e^{i\phi} \tag{2}$$

The Fourier analysis of the AC voltage $\underline{V}(\omega)$ allows for the superposition of sinusoidal source functions. The sum of individual sinusoidal solutions results in the solution of any periodic source. Therefore, knowing a sinusoidal source's solution is sufficient for all time-dependent sources [8].

2.1.2 Resistors

Ohm's law states that a voltage V applied over a conductor results in a current I proportional to the ohmic resistance R of the conductor. Electrical components with a constant resistance are known as resistors [8], and follow the equation:

$$V(t) = R \cdot I(t) \qquad \underline{V}(\omega) = R \cdot \underline{I}(\omega) \tag{3}$$

Since a resistor has a real value ohmic resistance R, the time-dependent voltage $V(t)$ is necessarily in phase with the time-dependent current $I(t)$. This also applies for the Fourier

transformation of both, $\underline{V}(\omega)$ and $\underline{I}(\omega)$.

2.1.3 Capacitors

Before discussing the AC response of a capacitor, let us first reiterate what a capacitor is. the classic capacitor consists of two opposing conducting surfaces. Inducing a charge on one of these surfaces, results in opposite charge carriers being induced on the other surface, caused by a phenomenon known as influence. Suppose both surfaces are connected to a source and ground respectively, a voltage V proportional to the amount of charge Q can be measured [9].

$$Q(t) = C \cdot V(t). \tag{4}$$

The proportionality constant C is known as the capacitance of the capacitor. It depends on the surfaces' geometries and material and is therefore a property of the component used.

Considering a simple circuit with an AC source and a single capacitor, the current can be solved for by looking at the time-dependent changes in the charge, resulting in the following equation:

$$I(t) = \frac{dQ}{dt} = C\frac{dV}{dt} = CV_0\frac{d}{dt}e^{i(\omega t+\phi)} = i\omega CV_0 e^{i(\omega t+\phi)}. \tag{5}$$

The value of the current in relation to the original voltage is $\underline{I}(\omega) = i\omega C\underline{V}(\omega)$. The voltage-current relation of a capacitor can be summed up in the following equation, where $Z_C(\omega)$ is known as the complex impedance of a capacitor.

$$\underline{V}(\omega) = Z_C(\omega) \cdot \underline{I}(\omega) \qquad\qquad Z_C(\omega) = \frac{1}{i\omega C}. \tag{6}$$

The real component of the Impedance $Z_C(\omega)$ acts as a variable resistance inside a capacitor controlled by the frequency of the applied AC voltage. This factor is rather big at low

frequencies and vice versa. With rising frequency the current increases for the same voltage. Rewriting the complex factor 1/i shows that it is equivalent to a phase shift of $\pi/2$. This means that the voltage is lagging behind the current [8].

2.1.4 Inductors

The classic inductor consists of an isolated wire wound into a coil. An electrical current flowing through this wire results in a magnetic field surrounding it. Through a phenomenon known as induction, this change in the magnetic field results in a voltage being induced inside the wire. This voltage is proportional to the change in current with a factor given by the component's physical properties known as its inductance L.

$$V(t) = L\frac{d}{dt}I(t). \tag{7}$$

The voltage-current relation can be solved by applying an AC source and integrating to receive an expression for the current I.

$$V_0 e^{i(\omega t+\phi)} = L\frac{dI}{dt} \Rightarrow I(t) = \frac{V_0}{L}\int e^{i(\omega t+\phi)}\,dt = \frac{V_0}{i\omega L}e^{i(\omega t+\phi)}. \tag{8}$$

The value of the current is the original voltage V_0 divided by the constant ωC. The voltage-current relation of an inductor can be summed up in the following equation, where $Z_L(\omega)$ is the complex impedance of an inductor.

$$\underline{V}(\omega) = Z_L(\omega)\cdot\underline{I}(\omega) \qquad\qquad Z_L(\omega) = i\omega L. \tag{9}$$

Similar to the capacitor, the real value of the impedance $Z_L(\omega)$ acts as a resistance controlled by the frequency of the applied AC voltage. This factor ωL is opposite the capacitive reactance in the way that it's rather small at low frequencies and vice versa. With rising frequency, this factor becomes increasingly bigger, and the current decreases for the same

voltage. The complex factor i can be interpreted as a phase shift of $-\frac{\pi}{2}$, meaning that the voltage is ahead of the current [8].

2.1.5 Kirchhoff's Laws

In addition to the components' properties, Kirchhoff's laws are fundamental to the discussion of circuits. They are mathematically used to predict voltage and current distribution over an electrical circuit. They state:

- Kirchhoff's current law: The sum of currents entering a certain point on a circuit is equivalent to the sum of currents leaving (see figure 3a):

$$\sum_i I_i = 0$$

- Kirchhoff's voltage law: The sum of changes in voltage over a closed path in a circuit is always zero(see figure 3b):

$$\sum_j V_j = 0$$

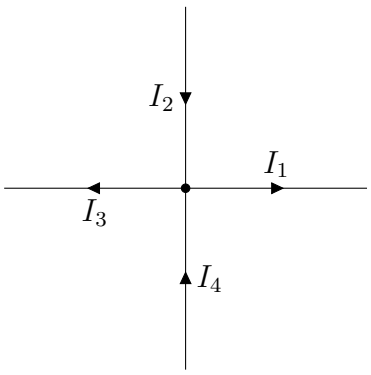

(a) Graphic illustrating Kirchhoff's current law. The sum over the currents I_i is zero

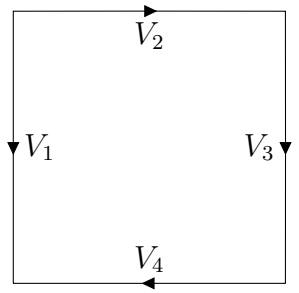

(b) Graphic illustrating Kirchhoff's voltage law. The sum over the voltages V_j is zero.

Figure 3: Illustration of Kirchhoff's current and voltage laws

2.2 Theory of Low-Pass Filters

The circuit for low-pass filters is the same as for voltage dividers, with components being changed to achieve the desired frequency response. To understand the relation of input voltage V_{in} to output voltage V_{out} the functionality of voltage dividers is the topic of the following sub-chapter.

2.2.1 Voltage Divider

Figure 4 shows a simple voltage divider, consisting of a voltage source V_{in} connecting to ground via two separate components. The output voltage V_{out} is measured across the second component.

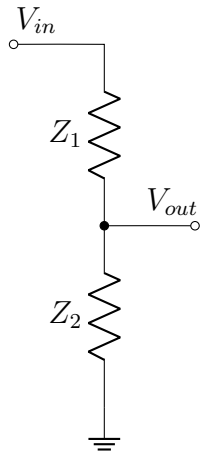

Figure 4: Voltage divider circuit made up of two impedances in series. Z_1 and Z_2 are components with unspecified impedance values. V_{in} and V_{out} are taken as measurements from the specified points to ground [10].

Applying Kirchhoff's Laws to this schematic results in equations for the total voltage and current relations.

$$V_{in} = V_1 + V_2 \qquad I_{in} = I_1 = I_2 = I_{out} \qquad V_2 = V_{out}. \tag{10}$$

V_1, V_2, I_1 and I_2 are the voltages and currents measured over the respective impedances Z_1 and Z_2. Ohm's law for impedances results in the following equations:

$$V_1 = Z_1 \cdot I_1 \qquad V_2 = Z_2 \cdot I_2 \qquad V_{in} = Z_{tot} \cdot I_{in}. \tag{11}$$

Because of the linearity of Ohms law impedances in series can be summed up to gain the total impedance Z_{tot}. Together with equations 10 and 11 the relation between V_{in} and V_{out} solely depending on the impedance can be calculated.

$$V_{out} = V_2 = Z_2 \cdot I_2 = Z_2 \cdot I_{in} = Z_2 \cdot \frac{V_{in}}{Z_{tot}} = V_{in} \cdot \frac{Z_2}{Z_1 + Z_2}. \tag{12}$$

Equation (12) illustrates that V_{out} is dependent on the ratio of Z_2 to $Z_1 + Z_2$. Increasing Z_1 therefore is the main contributor to lowering V_{out}. Meanwhile Z_1 only determines how big a change in Z_2 influences the attenuation of the signal.

2.2.2 Frequency Response of RC-Filters

A passive low-pass filter (also known as an RC filter, based on the components used) is a circuit designed to attenuate higher-frequency signals and pass signals of low frequencies. Passive filters are filters consisting of passive components (resistors R and capacitors C), which do not require an external source. There is no signal gain because there are no amplifiers with passive components. Therefore, the output level of passive filters is always lower than the input ($|\underline{G}| < 1$, $G_{\mathrm{dB}} < 0$, see equation (14)) [11].

To achieve the desired function of filtering higher frequencies the already discussed voltage divider only needs to be altered slightly. The first component remains a resistor with resistance R while the second component is switched with a capacitor with the impedance Z_C. This is done because, as Chapter (2.1.3) discussed, the capacitor minimizes current at low frequencies. Therefore almost all of the signal can be measured at the output and close to none is lost to the ground. Meanwhile, higher frequencies can pass the capacitor. More current can flow into the ground and the filter loses its output. The circuit of the RC filter can be seen in figure 5.

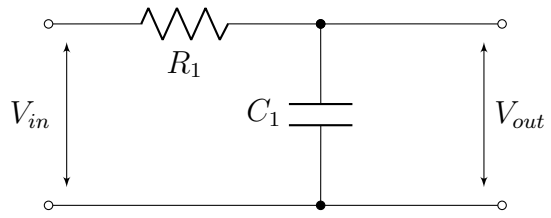

Figure 5: Layout of a typical 1st order RC filter. R_1 and C_1 are the resistance and capacitance of the components . V_{in} and V_{out} are measured in between the two arrows respectively.

Inserting Equation 6 and the impedance relation for resistors $Z = R$ results in the following equation for low pass filters:

$$\frac{V_{out}}{V_{in}} = \frac{\frac{1}{i\omega C}}{R + \frac{1}{i\omega C}} = \frac{1}{1 + i\omega RC}. \tag{13}$$

This equation contains the information on the magnitude and phase of the resulting output. To interpret this equation, the amplitude can be accessed via the absolute amount. At the same time, the phase shift is available through the geometric equation $\phi = \arg(z) = \arctan(\mathrm{Im}(z)/\mathrm{Re}(z))$. Instead of the output voltages being measured in volts, the attenuation of a filter is given by the gain $\underline{G}(\omega)$ or the gain in decibels G_{dB}. The relations are set through the following equations:

$$|\underline{G}(\omega)| = \frac{|V_{out}|}{|v_{in}|} = \frac{1}{\sqrt{1 + (\omega RC)^2}} \qquad G_{\mathrm{dB}}(\omega) = 20 \cdot log\left(|\underline{G}(\omega)|\right). \tag{14}$$

$$\phi = \arg(\underline{G}(\omega)) = -\arctan(\omega RC). \tag{15}$$

Plotting equations (14) in dependence of the frequency on a logarithmic scale results in the graphs shown in figure 6 (also known as "Bode plot").

An important point for describing the graph of a low-pass filter is the "cut-off" or "corner" frequency f_c. It is defined as the point where resistance and the absolute impedance of the capacitor are equal ($R = |Z_C| = 1/\omega C$). When this occurs the output signal is attenuated

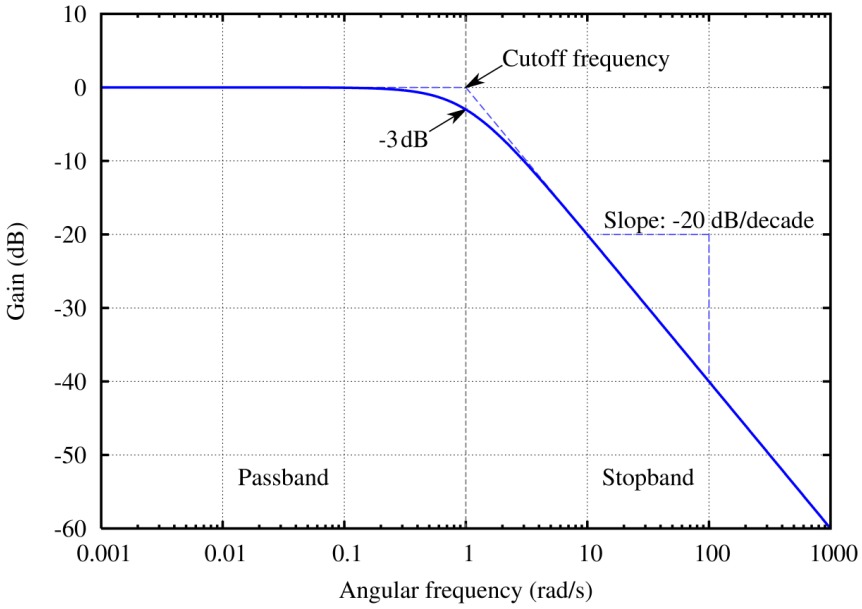

Figure 6: Bode plot of a 1st-order low-pass filter, showing the relation between attenuation and the frequency. The plot is divided into pass and stop band by the cut-off frequency f_c, with a roll-off slope of $-20\,\mathrm{dB/Decade}$ at higher frequencies [12].

by a factor of $1/\sqrt{2}$ times the input signal which is equivalent to $-3\,\mathrm{dB}$. The region before this point is known as the filter's pass band zone and has little to no attenuation. After the cut-off frequency, the signals are part of the so-called stop band where they are gradually attenuated with a roll-off slope of $-20\,\mathrm{dB/Decade}$.

As the filter contains a capacitor the phase shift ϕ lags behind the input signal as described in equation (14). With a DC-voltage, the lag is zero with it gradually rising with increasing frequency up to 90°. The cut-off frequency marks the spot where this phase shift is exactly 45° [11]. This response can be seen in figure 7.

The value of the cut-off frequency is solely set by the value of the electrical components. The equation is derived from the definition of cut-off frequency and capacitive reactance.

$$V_{out} = V_{in} \cdot \frac{1}{\sqrt{2}} \Rightarrow |Z_C| = R \Rightarrow R = \frac{1}{\omega C} \Rightarrow f_c = \frac{1}{2\pi RC}. \tag{16}$$

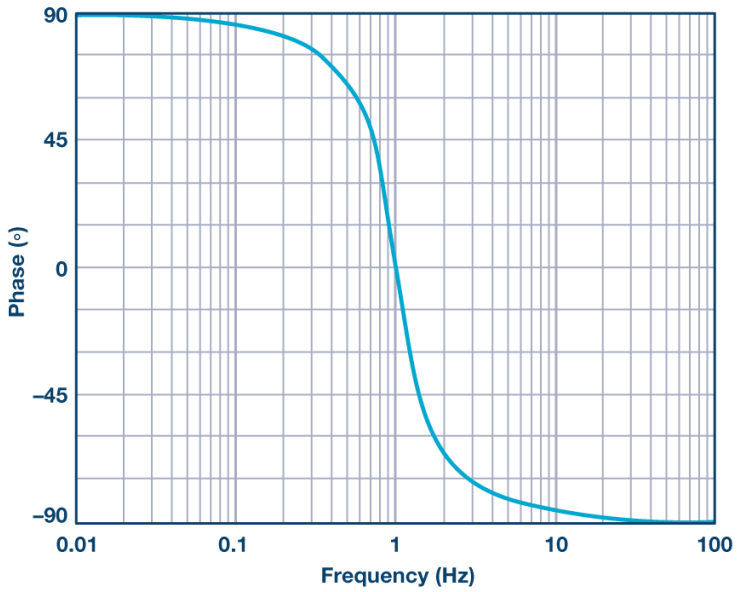

Figure 7: Bode plot of a 1st-order low-pass filter, showing the relation between phase and the frequency. [13].

2.2.3 Higher Order RC-Filers

Thus far, only first-order RC filters have been discussed. This arrangement with only a single resistor and capacitor can achieve a roll-off slope of $-20\,\mathrm{dB/Decade}$. In some filter circuits, having a steeper slope to remove unwanted signals can be advantageous, requiring higher-order filters. To create an n^{th} order filter, n such first order filters are cascaded in series, resulting in a slope of $n \times -20$ dB/Decade [11].

The disadvantage of higher-order filters is that many problems can arise with rising complexity. Higher filter orders need more space and lead to more tracks on a printed circuit board (PCB). This increased complexity would make our design more susceptible to parasitic effects between tracks and components. These can lead to an earlier reentrance of the filter (see Chapter 2.4.4). Another issue is that with rising order the overall resistance usually increases. This leads to lower currents and therefore a bigger loss of energy in the form of heat dissipation. An exact temperature measurement is important when doing noise experiments. Therefore with increasing order of the filter problems could arise in carefully controlled cryostat. In an ideal case, energy loss would not be a problem since at $0\,\mathrm{Hz}$ there is no loss in voltage ($V_{in} = V_{out}$), because there is no current flowing via the capacitor.

Since real components are imperfect in function this relation is not entirely the case at DC voltage. Including more stages only increases the effects mentioned above. When certain measurements are made over resistance to ground, the resistances of the filter can function as part of a voltage divider and decrease the overall transferred voltage. This is further elaborated in Chapter (2.3.1) Therefore we opted for a second-order filter which is a good trade-off between loss of transfer and the steepness of the slope.

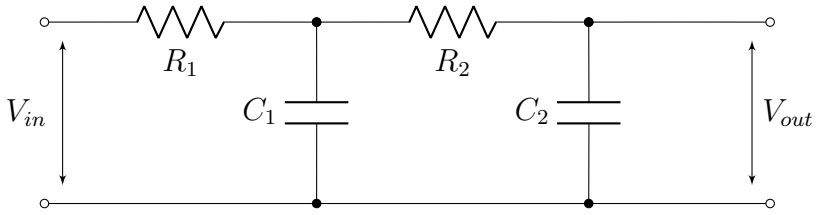

Figure 8: Layout of a typical 2nd order RC filter, consisting of two first order filters in series. R_1, R_2, C_1, and C_2 are the resistances and capacitances of the designated stage. V_{in} and V_{out} are measured in between the two arrows respectively.

Figure 8 shows the typical construction of a second-order low-pass filter. The output voltage of the first RC stage is directly used as the input voltage of the second RC stage, attenuating the signal further. In a filter with two times the same filtering stage in series, using the definition for the cut-off frequency that was used above ($R_1 = C_1 = R_2 = C_2$), leads to an attenuation of $V_{out} = 1/\sqrt{2} \cdot 1/\sqrt{2} \cdot V_{in} = 0.5 \cdot V_{in}$ or $-6\,\mathrm{dB}$ of the input signal at the cut-off frequency. In this case, the cut-off frequency is given by the following equation [11]:

$$f_c = \frac{1}{2\pi\sqrt{R_1 C_1 R_2 C_2}}. \tag{17}$$

As the roll-off slope of the filter increases with rising order, the $-3\,\mathrm{dB}$ point shifts to lower frequencies, and its pass band frequency changes. The shift can be calculated through the following equation and is visualized in figure 9 [11]:

$$f_{-3\mathrm{dB}} = f_c\sqrt{2^{(\frac{1}{n})} - 1}. \tag{18}$$

f_c is the calculated cut-off frequency, n is the order of the filter and $f_{-3\mathrm{dB}}$ the new $-3\,\mathrm{dB}$ pass band frequency. The frequency response of higher order filter is visualized in figure 9.

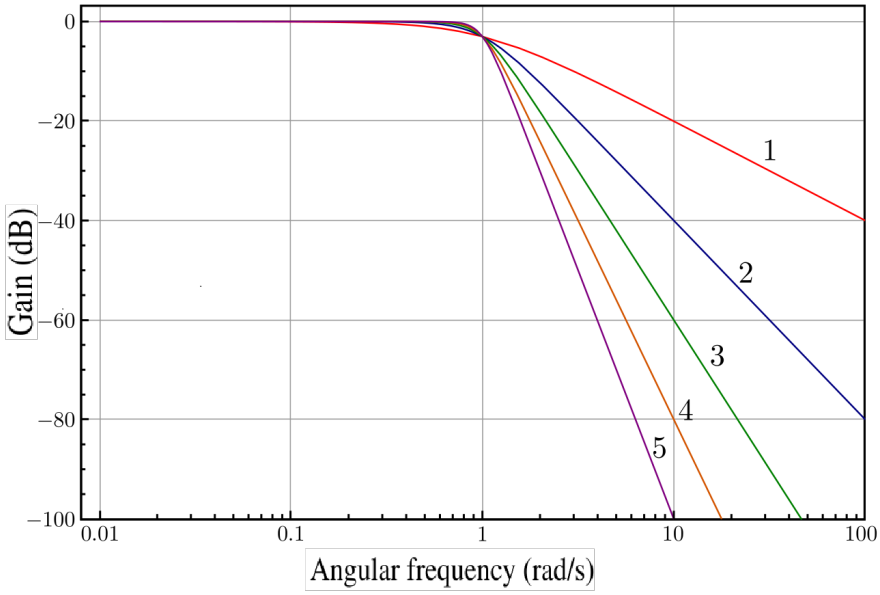

Figure 9: Bode plot comparing higher order (1 to 5) RC filters frequency response. The frequency is given in angular frequency $\omega = 2\pi f$ [14].

The right values and distribution of the components depend highly on the rest of the circuit connected to the filter, which will be discussed in the upcoming chapters.

2.3 Measuring Equipment

To test the frequency response of the different filters a lock-in amplifier and a vector network analyzer (VNA) have been used. All of the measurements in chapters 2, 3, and 4 were taken using both a VNA and a lock-in amplifier depending on the frequency range needed. Both these devices will be explained in the following two subchapters.

2.3.1 Lock-In Amplifier

The lock-in amplifier is an instrument used to detect very small AC signals. They are built on a principle called phase-sensitive detection (PSD), to single out a signal at a specific frequency and phase. The lock-in amplifier generates its internal reference signal $V_r \sin(\omega_r t + \theta_r)$ with its angular frequency ω_r. An outside signal is compared to this reference by using the orthogonality of sine functions. The lock-in amplifier multiplies the signal $V_s \sin(\omega_s t + \theta_s)$ with the reference, resulting in the following output of the PSD [15]:

$$
\begin{aligned}
V_{\mathrm{PSD}} =& V_r V_s \sin(\omega_r t + \theta_r)\sin(\omega_s t + \theta_s) \\
=& \frac{1}{2} V_r V_s \cos((\omega_r - \omega_s)t + \theta_r - \theta_s) - \frac{1}{2} V_r V_s \cos((\omega_r + \omega_s)t + \theta_r + \theta_s)
\end{aligned} \tag{19}
$$

If the PSD output is passed through a low-pass filter the AC signals will be removed unless the reference angular frequency ω_r matches the frequency of the signal ω_s. The resulting DC signal is proportional to the signal amplitude V_s [15]:

$$
V_{\mathrm{PSD}} = \frac{1}{2} V_r V_s \cos(\theta_r - \theta_s) \tag{20}
$$

Using a second reference function with a phase shift of 90° results in a second output that's also proportional to the signal, but with a different phase response:

$$
V_{\mathrm{PSD2}} = \frac{1}{2} V_r V_s \sin(\theta_r - \theta_s) \tag{21}
$$

Using both these outputs as vector components allows for the determination of both the amplitude and the phase of the signal. Amplifiers in the lock-in allow for the detection of signals with very small amplitudes this way. Modern lock-in amplifiers use digital reference functions and allow for quick frequency sweeps up to 600 MHz [15].

2.3.2 Vector Network Analyzer

The vector network analyzer (VNA) is an instrument that is especially used for high frequencies. It measures the network parameters of an electrical network by analyzing the reflection and transmission of a signal. At high frequencies, electronic signals in a network show similar characteristics to electromagnetic waves. These waves get transmitted and reflected at the device under test (DUT) based on the impedance Z_D in comparison to the impedance of the transmission line (see also chapter 2.4.3) $Z_0 = 50\,\Omega$. The resulting signals get transferred to receivers and are measured to gain the reflection parameters S11, S22, and transmission parameters S12, S21 [16]. The transmission and reflection coefficient are dependent on the

impedance of the DUT based on the following equations:

$$R = \frac{Z_D - Z_0}{Z_D + Z_0} \qquad T = 1 - \frac{Z_D - Z_0}{Z_D + Z_0} \tag{22}$$

Knowing the impedance for a DUT, for example, by using a calibration kit, allows the removal of unwanted influences of cables or different parts of the setup. This is done via a reference to expected transmission coefficients. The VNA in our measuring setup was used to measure up to a frequency of 20 GHz, but VNAs can reach up to 1 THz [16]. Figure 10 shows how a DUT (filter in our case) would be measured using a VNA.

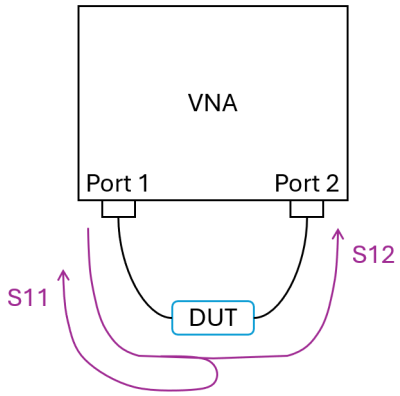

Figure 10: Schematic of DUT connected to a VNA. A signal is partially transmitted between port 1 and port 2 (S12) and partially reflected to port 1 (S11).

2.4 Design and Construction

The first step in designing an RC filter is finding suitable components for the right cut-off frequency. Based on our measurement system our goal is to achieve a cut-off frequency of around 10^4 Hz. This is highlighted in chapter 1. Equation (17) shows that this frequency is inversely proportional to the square root of both resistances and capacitance ($f_c \propto 1/\sqrt{R_1 C_1 R_2 C_2}$). Chapter (2.2.3) mentions that many problems can arise from choosing high resistances. Even if it does not affect the transfer in an ideal case, it will still result in power dissipation, since higher resistance leads to heat development in the circuit overall increasing thermal noise [4].

Furthermore, connecting a sample to the filter will add another resistance to the circuit. This leads to a voltage divider with a larger impact for larger resistance values. (Thus it is advantageous to choose lower values for the resistors.) The general influence of load resistance will be discussed in Chapter 2.4.1. To achieve a low cut-off frequency while minimizing the negative effects of high resistance, the capacitance should be maximized while the resistances are kept as small as possible. In the RC printed circuit boards (PCB) design, the surface mount devices (SMDs) 0603-size was used as a good equilibrium between optimal space efficiency and available high capacitance components. Here the highest commercially available capacitance is $C = 47\,\mathrm{nF}$. Consequently, the chosen resistance for a single-stage RC filter would be $R = 100\,\Omega$. To optimize the designing process of the RC filter, most test filters were first simulated using the software LTspice which allows the construction of electronic circuits giving the resulting amplitude and phase response. For further information refer to the official website of the company Analog Devices [17]. Figure 11 shows a simulation of a simple second-order RC-filter with the $-3\,\mathrm{dB}$ frequency around $10^4\,\mathrm{kHz}$.

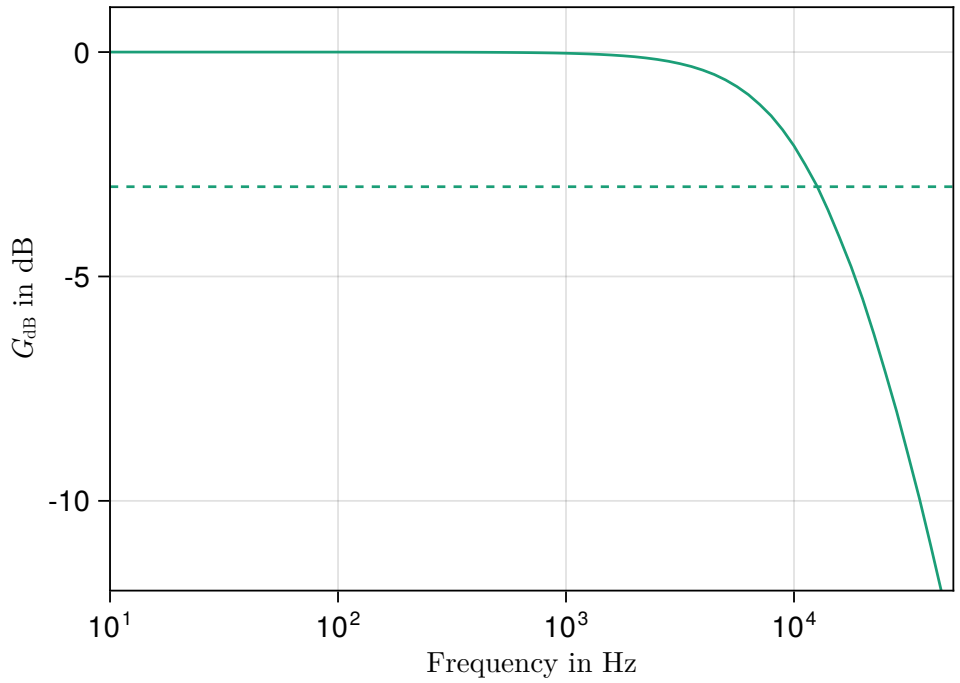

Figure 11: Bode plot of a second order RC filter simulated in LTspice. The resistances are $R_1 = R_2 = 100\,\Omega$. The capacitors are $C_1 = C_2 = 47\,\mathrm{nF}$. the $-3\,\mathrm{dB}$ cut-off frequency is shown by the dotted line and equals $f_{-3\mathrm{dB}} \approx 14\,\mathrm{kHz}$.

2.4.1 Loading Optimisation

The distribution of values must consider the effect of a loading resistance on the Bode plot of the filter. The loading resistance in question represents the load of the sample and adds to the measuring circuit in our case. The resistance of a sample can vary between $1\,\mathrm{k\Omega} - 500\,\mathrm{k\Omega}$ depending on its attributes. The cut-off frequency must stay consistent even with the highly variable load resistance to keep the setup as flexible as possible. Understanding the response of the filter to the load resistance is therefore focus of this chapter. Figure 12 shows the circuit used to simulate this effect.

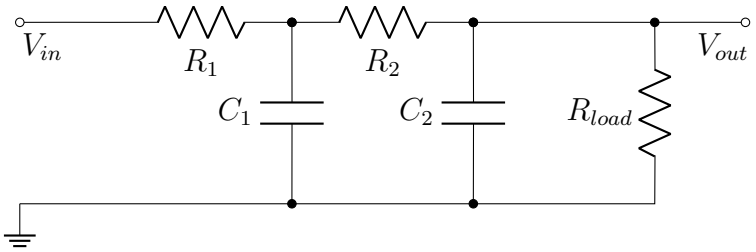

Figure 12: Circuit used to simulate the loading resistance. the resistances and capacitances of the circuit are given with R_1, R_2, C_1 and C_2. The resistance of the sample is simulated with R_{load}.

Figure 13 shows data simulated in LTspice, illustrating different loading resistances' influence on other distributions of the component's values. The green plots show the frequency response on a second-order RC filter where the components of both stages have equal values. The resistances are $R_1 = R_2 = 100\,\Omega$ and the capacitances are $C_1 = C_2 = 47\,\mathrm{nF}$. The orange plots illustrate the frequency response on a second-order RC filter where the values are distributed as follows. The resistances are $R_1 = 18.18\,\Omega$, $R_2 = 181.82\,\Omega$ and the capacitances are $C_1 = 85.45\,\mathrm{nF}$ and $C_2 = 8.55\,\mathrm{nF}$. The total resistance $R = R_1 + R_2$ and total capacitance $C = C_1 + C_2$ is equal for both setups, but $R_2 \approx 10\,R_1$ and $C_2 \approx 1/10\,C_1$ for the second setup. The simulation was done for $R_{load} = 1\,\mathrm{k\Omega}$ and $R_{load} = 500\,\mathrm{k\Omega}$ for each setup respectfully.

Low load resistance leads to overall decreased transfer. This happens because the load resistance acts as a frequency-independent connection to ground. The cut-off frequency (marked by squares in figure 13) shifts with loss in transfer. This change in frequency is known as the "loading effect". It can be suppressed by increasing the impedance of the

second RC filter stage, i.e. $R_2 > R_1$ and $C_2 < C_1$ [6]. It is therefore common to use RC filters where resistances and capacitances of the second stage are distributed as $R_2 = 10\,R_1$ and $C_2 = 1/10\,C_1$ respectively.

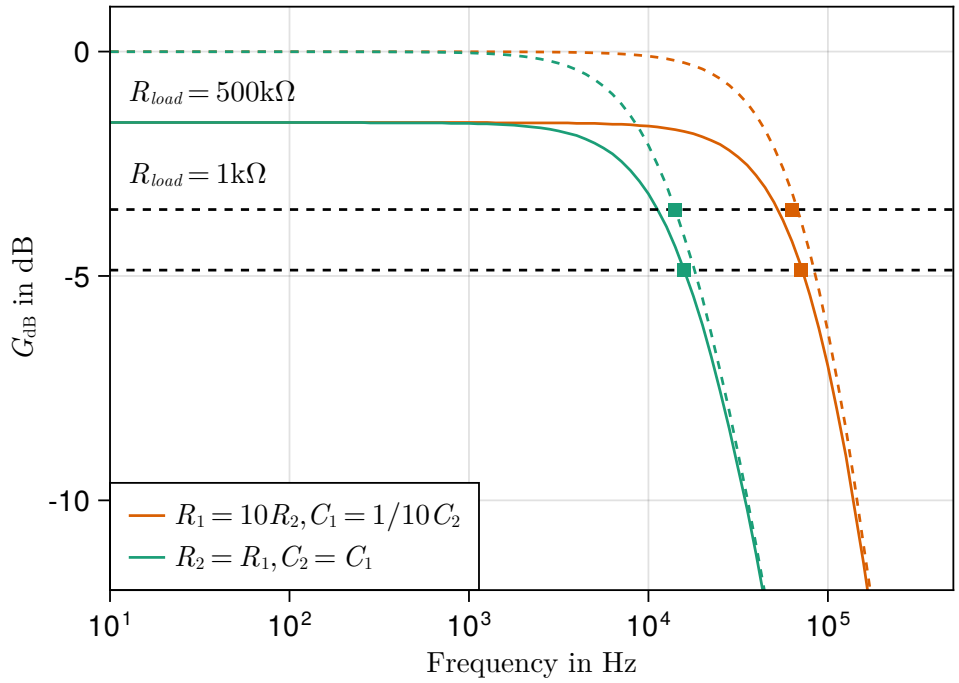

Figure 13: LTspice simulation of the transfer function of the filter shown in figure 12 for different load resistors $R_{load} = 1\,\mathrm{k}\Omega$ (dashed line) and $R_{load} = 500\,\mathrm{k}\Omega$ (full line). The total resistance and capacitance ($R = R_1 + R_2 = 200\,\Omega$ and $C = C_1 + C_2 = 94\,\mathrm{nF}$) are constant. The orange plot is a filter with an enhanced impedance for the second stage, while the green plot has the same impedance for the first and second stages, The cut-off frequencies are marked by squares.

The important takeaway in this test is the stability of the $-3\,\mathrm{dB}$ frequency $f_{-3\mathrm{dB}}$ with changing load resistance. The change in frequency $\Delta f_{-3\mathrm{dB}}$ between $1\,\mathrm{k}\Omega$ and $500\,\mathrm{k}\Omega$ in the LTSpice simulation is:

$$R_2 = R_1 : \ \Delta f_{-3\mathrm{dB}} \approx 7.7\,\mathrm{kHz}$$

$$R_2 = 10R_1 : \ \Delta f_{-3\mathrm{dB}} \approx 1.7\,\mathrm{kHz}.$$

The comparison shows an improvement in the stability of the cut-off frequency, with increased impedance for the second stage of the RC filter. However, the improvement seems too small to impact the functionality of the filter in noise measurement applications. Therefore, out of

convenience's sake, the choice was made to set resistors and capacitors to $C_1 = C_2 = 47\,\text{nF}$ and $R_1 = R_2 = 100\,\Omega$.

2.4.2 PCB design

The following circuit and PCB were designed with the software KICad. For further information refer to the official website [18]. Figure 14 shows the resulting circuit. The spaces for resistors and capacitors are marked with R1, R2, C1, and C2. The grounded part of the circuit is marked with "GND". J1 marks the connector to a coaxial cable, with (1) being the connection to the inner conductor with the input voltage V_{in} and (2) being the connection to the outer conductor that is on ground potential. The test point TP3 is the spot where the output voltage V_{out} is taken and is used in this circuit as a soldering point to attach further filtering stages (see Chapter 3).

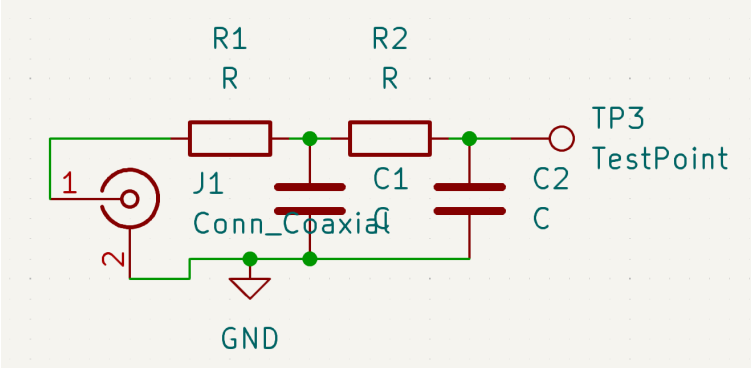

Figure 14: RC filter circuit designed in KICad. R1, R2, C1, and C2 mark the resistors and capacitors. J1 is a coaxial connector and TP3 is a test point used as a soldering plate. [18]

Figure 15 shows the final design of the PCB used in the filtering setup. The PCB is divided into front and back sides. The front holds all of the components while the backside is used to solder connectors. This allows for access to the components retroactively and therefore increases flexibility by making it possible to change up the components in the finished filter without taking it apart (see also Chapter 4.1). The inner conductor of a female SMA connector can be soldered to the metal plate centered on the left side of the back. The outer conductor of the SMA connector can be soldered to the four plates located at the corners on the left side of the front and the back of the PCB. The last connector on the back (TP3) is

used as a soldering spot to connect a copper wire used in the copper powder filter stage of the setup (see Chapter 3).

(a) Front of the PCB

(b) Back of the PCB

Figure 15: Final design of the PCB. The components are marked with the respective Symbol (see figure 14). The light green space is a conductive surface and sets the ground potential for most of the PCB. The front and back sides are connected via holes. The yellow surface is a soldering spot. The silver spots are soldering attachments to a female SMA connector. [18]

2.4.3 Influence of the Coaxial Cable

The influence of the measuring electronics is important to consider when looking at the frequency response of a filter. Since the filter will be placed inside the cryostat close to the sample, it will be connected to a nontrivial amount of coaxial cable. This type of cable is categorized by having its outer conductor, usually made of one to four layers of woven metallic braid, on ground potential surrounding the inner conductor that's on the desired voltage. Both conductors are separated by a dielectric material used as an insulator. This outer conductor functions as a shield, protecting the inner conductor from electric and magnetic fields on the outside [19] [20]. This proximity of conductors functions as a capacitor. In addition to this, the conductors have an in-series resistance. Therefore the coaxial cable essentially functions as an RC filter stage. Since the capacitance is distributed across the length of the coaxial cable, it would not be correct to simply implement a resistance and a capacitance, therefore modeling the cable as a single RC element. Instead, it can be advantageous to use a model known as a distributed line. Here the component is implemented with a finite length, where each "section" of the coaxial cable is modeled as having an infinitesimally small capacitance and resistance. The schematic for a section of a lossless distributed line can be seen in 16.

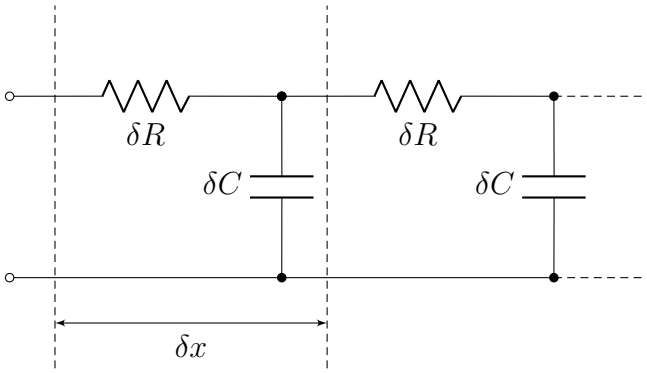

Figure 16: Schematic of a section of a lossless distributed line. A small section δx has a capacitance δC and resistance δR.

In the limit $\delta x \longrightarrow 0$, the absolute value of the gain $|G(\omega)|$ of such a line can be described through the following equation, by describing the voltage as a superposition of wave functions:

$$|G(\omega)| \propto e^{-k'' L} \tag{23}$$

L is the length of the coaxial cable, while $k'' = \mathrm{Im}(k)$ is the imaginary part of the angular wave number [8].

To simulate this influence the lossless transmission line (Tline) component was used in LTspice. The energy lost in real data is not simulated. In this application, the difference is minimal and therefore can be ignored [21]. Figure 17 shows the circuit used to simulate the inclusion of a coaxial cable. The technical information on the thermocoax was taken from the website of manufacturer BlueFors [22].

Figure 18 shows the Bode plot of the circuit shown in figure 17 in comparison to the simple second-stage RC filter with the same components (see figure 11). The transmission line functions similarly to another RC stage and decreases the cut-off frequency. With a capacitance of $C = 562\,\mathrm{pF}$ and a resistance of $R = 155\,\Omega$ the transmission line is only negligibly different from another RC filter stage with the same components.

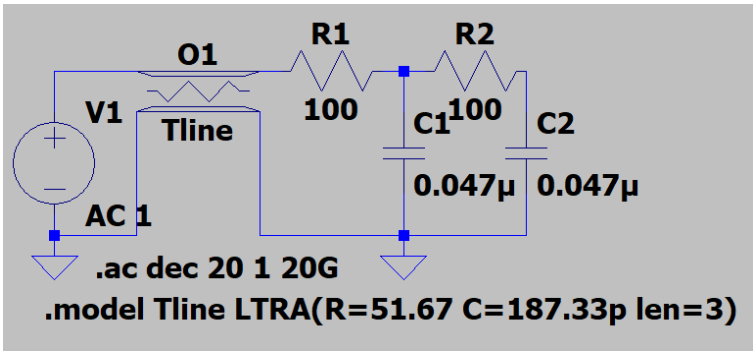

Figure 17: LTspice circuit of a second stage RC filter (see 11) with a transmission line (O1) between filter and voltage source. The transmission line has a resistance of a $R = 51.67\,\Omega/m$, a capacitance of $C = 187.33\,\mathrm{pF/m}$ and a length of $3\,\mathrm{m}$. The output voltage is taken in between R2 and C2.

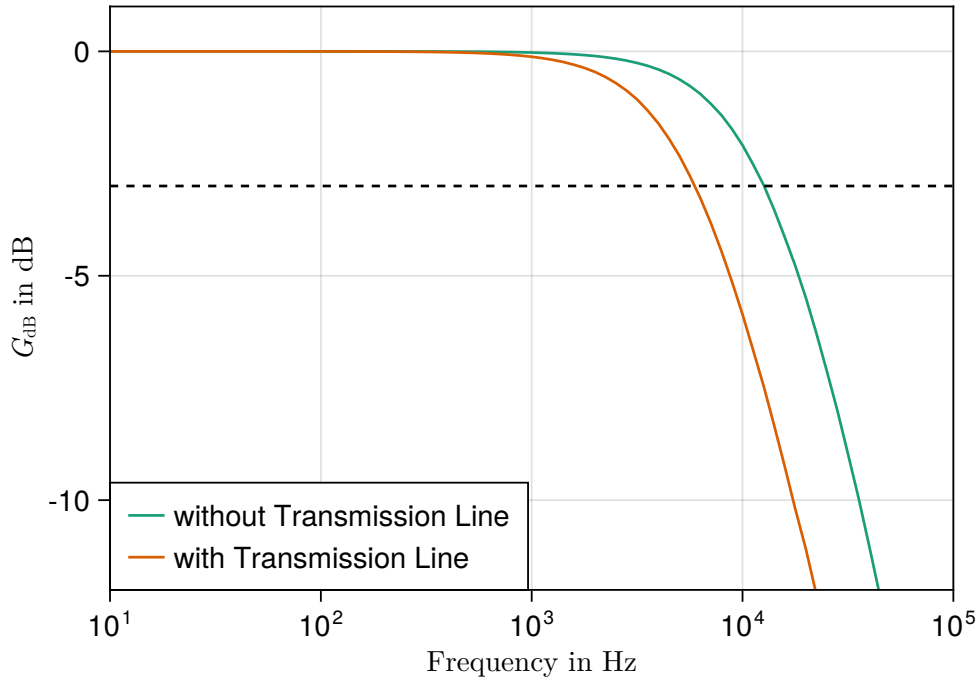

Figure 18: Comparison of an LTspice simulation of a second stage RC filter with and without implementing a transmission line. resistances and capacitances of the filter are $R_1 = R_2 = 100\,\Omega$ and $C_1 = C_2 = 47\,\mathrm{nF}$. The transmission line has a resistance of a $R = 155\,\Omega$ and a capacitance of $C = 562\,\mathrm{pF}$

2.4.4 Reentrance in non-ideal RC-filter

The ideal RC filter only exhibits increasing attenuation with rising frequency. This is not the case with real RC filters, because of imperfections of the real components. With rising

frequency, components like capacitors and inductors especially start to deviate from their ideal model.

An ideal capacitor stores and releases electrical energy without dissipation. In practice though capacitors have impurities in their dielectric, leading to undesired effects that are especially noticeable in the high frequencies response of a capacitor [8]. To model this deviation, it is practical to use several other ideal components.

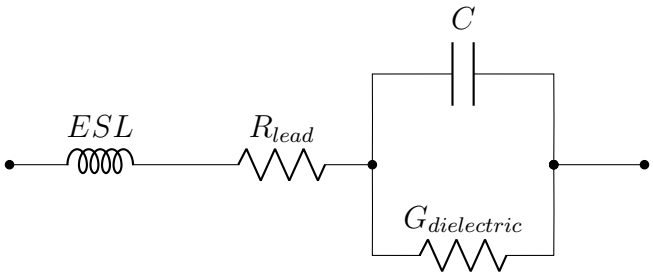

Figure 19: Equivalent circuit of a real capacitor with capacitance C. the in-series resistance is given with R_{lead}, the parallel resistance with $G_{dielectric}$ and ESL is the equivalent series inductance of the component.

Figure 19 shows one such equivalent circuit. The dissipation is simulated with two different resistances that lead to increased impedance. R_{lead} is the resistance of the connection between the component and the circuit as well as the intrinsic resistance of the circuit. The conductance $G_{dielectric}$ is parallel to the capacitance and accounts for the imperfect dielectric material. It allows for a small leakage current that simulates the slow discharge of the capacitor over the dielectric material. At high frequencies, capacitors also gain an inductive component, simulated here as "ESL" (Equivalent series inductance) [8]. According to the manufacturer Reichelt Electronics SMD capacitors have insulation resistances in the magnitude of $10^{10}\,\Omega$ and the tolerance for the capacitance is around 10% [23]. The ESL of SMD capacitors is in the range of $10^{-9}\,\mathrm{H}$ [24]. Finding a comparable value for the lead resistance can be difficult since it depends on the amount of solder paste, the footprint used for the PCB design, and the component itself. Comparable tests found lead resistance values of around $10^{-4}\,\Omega$ [25].

In addition to the real capacitor, other effects are present when looking at real RC filters made on PCBs. Due to the proximity of the components, certain influences between the

different tracks of the PCB can be modeled as a connection over a capacitor. The tracks of the PCB itself have an inductance, that is around 10^{-10} H per mm [26], as well as a resistance around $10^{-4}\,\Omega$ per mm [27].

All these effects together lead to a phenomenon known as reentrance for the RC filter. With rising frequencies, the inductances have a bigger impact and the filter starts to function as a band stop filter instead of a low pass filter. Figure 20 shows the measured Bode plot of the RC filter designed in chapter 2.4.2 in comparison to a simulation of the equivalent circuit with real components. The circuit is shown in figure 21.

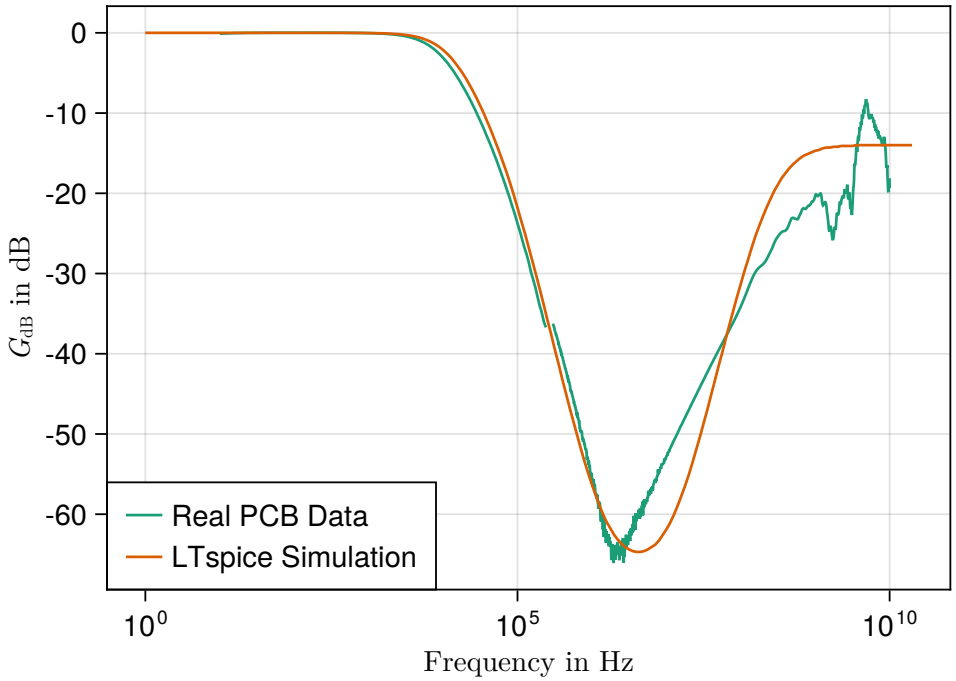

Figure 20: Comparison of Bode plots between a LTspice simulation (see figure 21) and the measured PCB shown in figure 15. The reentrance caused by the real components of the filter is seen at around 10^6 Hz. The filter gains in transfer at a rate of about 20 dB/decade

An LTspice simulation allows a simple recreation of the measured Bode plot. A lot of different components can be involved in the equivalent circuit. Hence there is no description of the parasitic values of the components from the manufacturer a lot of the possible fit parameters are unknown. We have abstained from fitting the data, but a similar reentrance can be simulated, for example with the circuit shown in figure 21. The inductors play the most important role, as their values dictate the frequency range of the bandpass filter when

set in series with the capacitors (L3 = L4 = 30 nH), and L1 = L2 = 30 nH dictate the total transfer for frequencies higher than approximately 10^9 Hz in this case. With an error of around $\Delta L = \pm 10$ nH using these values for a simulation results in a comparable reentrance frequency. Comparing these values to the values of typical ESL for SMD components and PCB traces shows that they are bigger than expected by a factor of about 10 [24] [26].

The resistors R3 = R4 = 2.5 Ω, with an error of $\Delta R = \pm 1\,\Omega$ set a depth of the minimum comparable to the measured reentrance when used in the simulation. Comparing this to typical values of resistances in PCB circuits the value is still bigger than expected by a factor of around 10 [25] [27].

The simulation is not a close fit to the measured data but can illustrate the changes in components with higher frequencies. The values that result in a comparable frequency response are far greater than expected. This indicates that the equivalent circuit is more complex than the one used for the simulation (see figure 21).

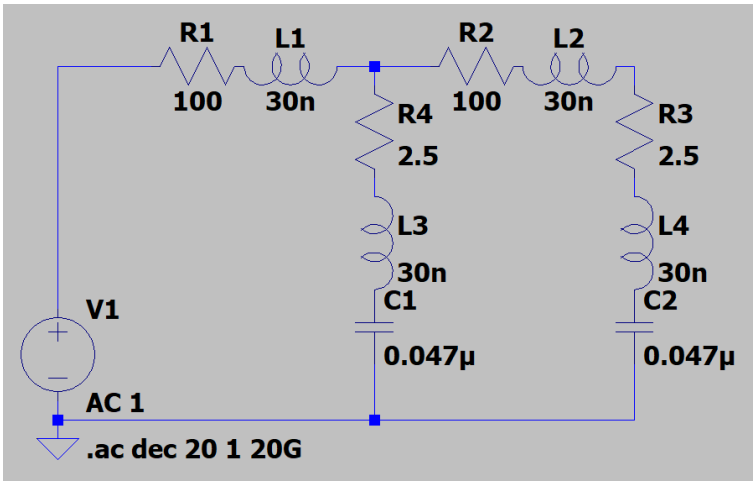

Figure 21: LTspice circuit of an RC filter ($R1 = R2 = 100\,\Omega$ and $C1 = C2 = 47$ nF) with added inductance in series with every component ($L1 = L2 = L3 = L4 = 30$ nH) and resistances for the capacitors ($R3 = R4 = 2.5\,\Omega$).

3 Copper Powder-Filter Stage

A practical way of reducing the influence of high frequencies is through the use of eddy currents in the wire. The equivalent filters are known as metal powder filters. Almost all metals can be used in the process of creating such a filter, although copper is most often used. Suspending copper powder in epoxy creates a cheap and easy way to introduce another filtering stage that can effectively attenuate even higher frequencies than the RC filter, especially due to the reentrance of the RC filter. The following chapters introduce the physical effects the filter is built upon as well as the optimizations made and ultimately the finished design implemented together with the RC filter stage discussed in chapter 2.

3.1 Theory of Metal Powder Filters

The focus of this first chapter lies in the introduction of the theories that are fundamental in understanding how a simple copper powder filter can be used as an effective filtering stage.

3.1.1 Eddy Current

Per the Maxwell-Faraday equation,

$$\nabla \times \mathbf{E} = -\frac{\partial \mathbf{B}}{\partial t}, \tag{24}$$

a time-dependant magnetic field $\mathbf{B}$ results in a circular electric field $\mathbf{E}$. Moving a conductor through a magnetic field changes the magnetic flux flowing through the conductor at the edges of the magnetic field. Given a point on the conductor, the magnetic flux increases as it gets nearer to the magnet. This change in flux $-\partial\mathbf{B}/\partial t$ creates a circular electrical field in the conductor. This field creates a counterclockwise flow of electrical current known as an eddy current.

By Lenz's law, the eddy current creates a magnetic field that opposes the changing magnetic field. Thus eddy currents react back on the source of the magnetic field and dampen the change [9].

3.1.2 Skin Effect

A current in a conductor creates a magnetic field in and surrounding the conductor. Applying an AC across the conductor results in a changing current intensity inside the conductor and therefore also a changing magnetic field. The resulting eddy currents create a counteracting field known as the counter-electromotive force (back EMF). The back EMF is strongest at the center of the conductor, allowing the current to only flow near the surface of the conductor, thus increasing the effective resistance of the conductor. This effect is known as the skin effect. The alternating current density J is highest at the skin of the conductor with it exponentially decreasing towards the center, given by the following equation:

$$J(d) = J_s\, e^{-(1+i)d/\delta} \tag{25}$$

J_s is the AC density at the surface of the conductor and d the depth. The imaginary part of the exponent accounts for the increasing phase shift with depth. The skin depth δ is hearby defined as the decay length of the exponential equation. The skin depth depends on the frequency f of the AC, and the materials resistivity ρ and magnetic permeability μ [28]:

$$\delta = \sqrt{\frac{\rho}{\pi f \mu}}. \tag{26}$$

This decrease in skin depth can be used for skin effect damping. A conductor is submerged in a metal powder. At high frequencies, the current mainly flows at the conductor's surface. The overall resistance increases leading to increased dissipation. Due to the vast surface of metal powders compared to the bulk, one expects an enormous dissipation caused by the skin effect. The effective resistance and thus the absorption of signals increases with rising frequency. Conversely, there is little to no effect at low frequencies making this effect perfect for filtering high frequencies [29].

3.2 Design and Construction

Metal powder filters are made as follows. A metal wire of usually $1 - 3\,\mathrm{m}$ is wound up and mounted in a box, with the ends soldered to connectors. The box is then filled with a mixture of metal powder and epoxy. The epoxy is liquid and therefore useful in distributing the powder and making it easy to fill the space surrounding the wire. After hardening, the epoxy helps to dissipate the heat from the grains to the environment.

The resulting design can be seen in figure 22. Two female sub-miniature version A (SMA) connectors are mounted at either side of a copper box with the dimensions $50\,\mathrm{mm} \times 13.06\,\mathrm{mm} \times 9.46\,\mathrm{mm}$ and a thickness throughout of $1.5\,\mathrm{mm}$. An insulated copper wire with a diameter of $100\,\mu\mathrm{m}$ is soldered to the inner conductor of the connectors on both sides. The connectors are soldered (later bonded with silver epoxy) to the box to function as a ground plane and give a good thermal connection throughout the filter. The copper powder epoxy mixture is made by mixing $3.2\,\mathrm{g}$ Stycast ($2.5\,\mathrm{g}$ part A and $0.7\,\mathrm{g}$ part B) with $7\,\mathrm{g}$ copper powder. The copper powder used, the length of the wire, and different design choices will be discussed in Chapter 3.3.

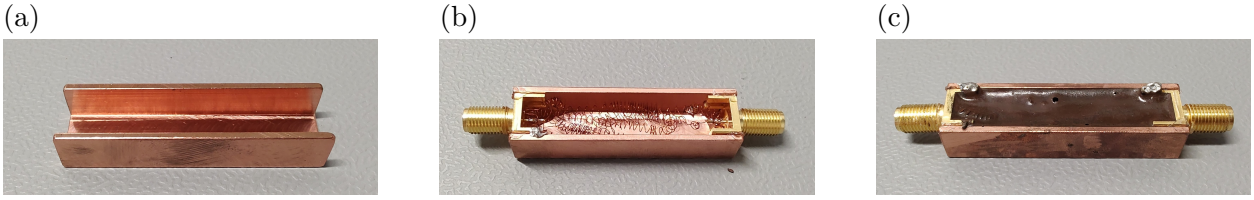

Figure 22: Three design stages of the copper powder filter. a) A simple copper box with dimensions 50mm × 13.06mm × 9.46mm and thickness of 1.5mm. b) A copper box with added wire, connecting the inner conductor of two SMA connectors. c) A copper box with wiring, filled with a copper powder (7 gram) and stycast (3.2 gram) mixture.

Figure 23 shows the frequency response of a simple copper powder filter with and without applying the powder epoxy mixture. Visible at high frequencies around $10^9\,\mathrm{Hz}$ and beyond, the copper powder makes a difference in attenuation of around $-20\,\mathrm{dB}$.

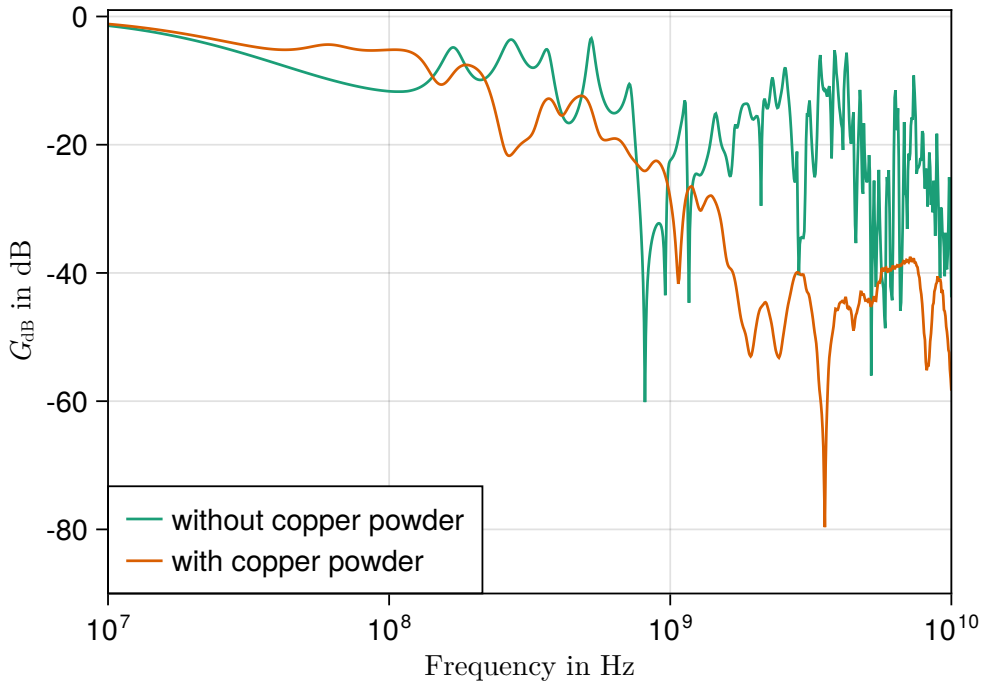

Figure 23: Bode plot of the filter shown in figures 22b and 22c. The length of the wire is 1.5 m. Data was measured with a network analyzer (VNA).

3.2.1 Optimization

At high frequencies, a lot of factors can impact the quality of the Bode plot of copper filters. For example, stray capacitance and resonances have a big effect on the high-frequency response of copper powder filters. This is enhanced by the fact that the transfer is measured on a logarithmic scale and is therefore strongly influenced by small changes in the outgoing voltage. This chapter therefore focuses on the two most important variables, being the chosen powder and the length and form of the wiring.

Referencing Chapter 3.1.2, a good way to increase the skin effect damping of the copper powder is by increasing its surface compared to its bulk. Using smaller grain sizes of powder has this effect and should therefore increase the attenuation of the copper powder filter.

Figure 24 shows a comparison of two different copper powders. One with a grain size of 37-53 µm, the other 37-88 µm. The difference in attenuation is relatively small, around -5 dB. Which filter has a higher attenuation is highly dependent on the frequency and seems to vary throughout. Small changes in the size of the grains therefore seem to be overshadowed

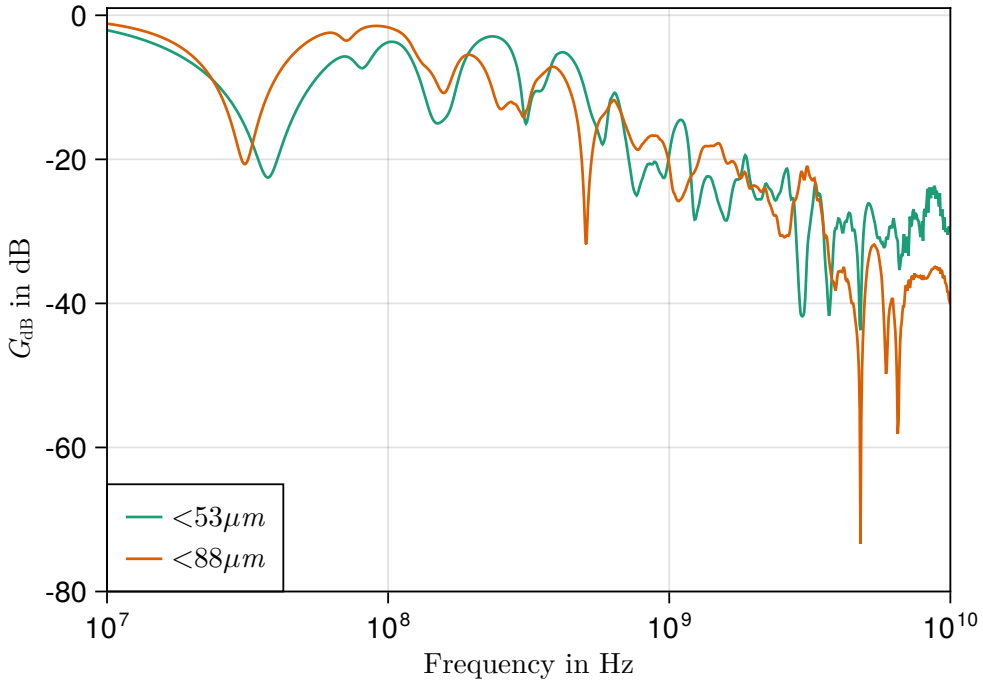

Figure 24: Bode plot comparing two different kinds of copper powders. The first powder (green plot) has a grain size of 37-53 µm, and the second (orange plot) has a grain size of 37-88 µm.

by other effects. The copper powder with a grain size of 37-53 µm will be chosen from here on out.

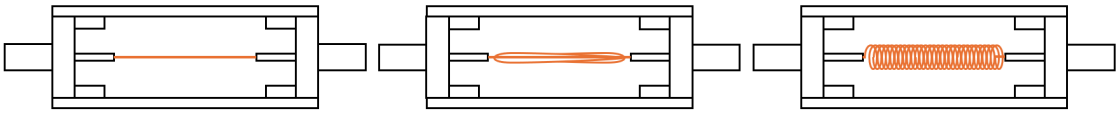

Figure 25: Different winding techniques for the copper powder filter. From left to right: straight line, laid back and forth and coiled.

Comparing different winding techniques as seen in figure 25 and wire lengths results in figure 26. The first thing to note is the characteristic peaks that are especially strong in the wire that is laid back and forth between the connectors. These peaks are a likely result of the resonance between different sections of the wire. The peaks and dips can be seen in previous filters as well. With high frequency, a straight section of the wire can function as an antenna and start emitting energy in the form of electromagnetic waves. Since the size of the antenna has to be in relation to the wavelength of the signal and therefore the frequency,

such emissions only happen at specific frequencies. Changing the form of the wire can also suppress this effect as can be seen with the green and orange plot. The second interesting thing to note is that with an increased length of wire, the attenuation is increased. The longest wire with 100 cm is most of the time up to 10 dB below the other lengths and reaches an attenuation of up to −80 dB. Therefore a 3 m wire, the longest wire compatible with the size of the box, will be used.

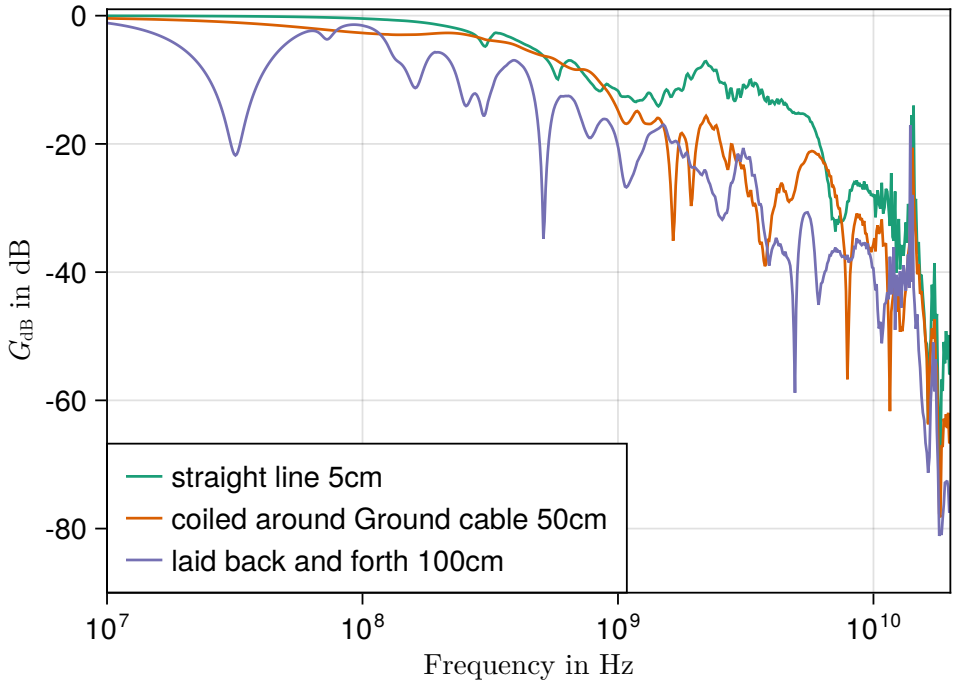

Figure 26: Bode plot comparing different wires. A 5 cm straight wire between the SMA connectors (green), a 50 cm wire that is coiled around a rode on ground potential (orange), and a 100 cm wire that is laid back and forth between the connectors (purple).

3.2.2 Stray Capacitance

Stray capacitance is the unavoidable capacitance between two parts of an electrical circuit simply caused by their proximity to one another. When two components are close to each other, they are affected by the other's electrical field and store opposite electrical charges like a capacitor. At low frequencies, these stray effects can mostly be ignored, but at high frequencies, it can be a major problem [30]. To test this effect over a copper powder filter, two SMA connectors were set in a copper case, omitting the cable between them, which

was then filled with the copper powder epoxy mixture with a ratio of 7 g copper and 3.2 g stycast. The resulting frequency response was then measured. To compare the transmission to the transmission via the air two SMA connectors were also set into a copper case and the transmission was measured without filling the copper case with any material. The resulting data can be seen in figure 27.

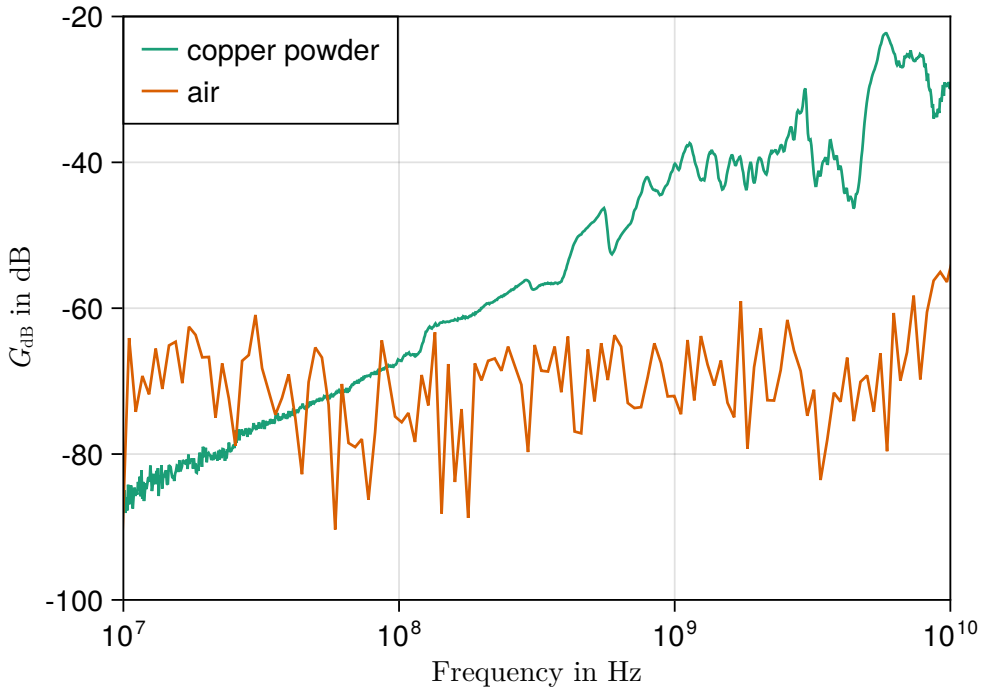

Figure 27: Comparison of the transmission via the copper powder and air at high frequencies.

The transmission via air a distance of about 4 cm is relatively constant around −70 dB. The transmission via the copper powder is lower at low frequencies but increases almost linearly with the frequency at a rate of around 20 dB/decade. The linear increase with the characteristic slope is similar to the Bode plot of a high pass filter. This could be the case since the copper powder between the SMA connectors functions as a capacitor at high frequencies. In addition to this, there is a high resistive connection to ground via the copper powder. Together this forms a circuit with an equivalent function to a high pass filter (see Chapter 2.2.1). With rising frequency the capacitor formed by the SMA connector becomes more conductive and the transmission increases. To reduce this transmission the design of the copper powder filter would need to be reevaluated. The stray capacitance therefore sets

a limit to the maximal achievable attenuation at high frequencies.

4 Application

The filter stages are set as close to the sample as possible, to reduce the outside magnetic influence on the experiment. Since the space in the cryostat is limited, only the RC filter and the copper powder can be situated below the mixing chamber. This point is situated right above the docking station of the sample and marks the point with the lowest temperature inside the dilution refrigerator. In contrast, the π-filter is located outside of the cryostat. Since the performance of different materials is different at RT compared to low temperatures ($\sim$ 10mK), the frequency response of the final filter will be analyzed at low temperatures in Chapter 4.2.

4.1 Final design

The joining of the two filter stages is rather easy. The finished PCB can be placed inside one of the SMA connectors and is soldered to the inner conductor as well as thoroughly connected to the outer conductors on ground potential. The wire of the copper powder filter stage is connected to the opposite end of the PCB. The connectors are mounted inside a copper box, as done with the copper powder filter (see figure 22). The connection between the SMA connectors and the box is done with silver epoxy to ensure a strong hold and a good thermal connection. The copper box is then filled with the copper powder epoxy mixture until all of the wire and the underside of the PCB are covered. A schematic of this design can be seen in figure 28.

Figure 29 shows a comparison between multiple test filters. The RC stage itself can be seen in the light green plot and shows the specific dip at 10^6 Hz to -60dB, with the characteristic reentrance afterward. Most wire lengths show only a slight improvement in attenuation above 10^6 Hz. At higher wire lengths around 250 cm the improvement becomes noteworthy with a plateau of around -80dB between 10^6 Hz and 10^7 Hz. The reentrance is far slower as well and doesn't reach the same height as with only the PCB. At around 2×10^{10} Hz most filters descend in attenuation again with the filter with 250 cm wire reaching as low as -80dB.

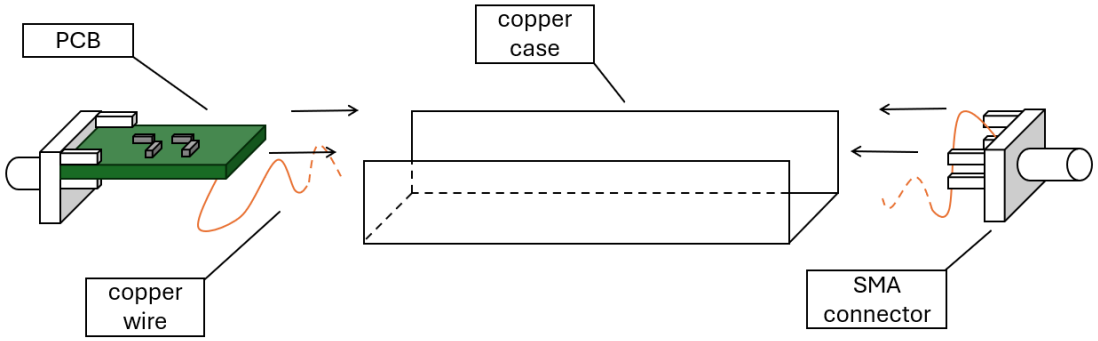

Figure 28: Schematic of final filter. Two SMA connectors, one with a PCB, are connected via a copper wire and placed inside a copper case. The case is then filled with a copper powder epoxy mixture.

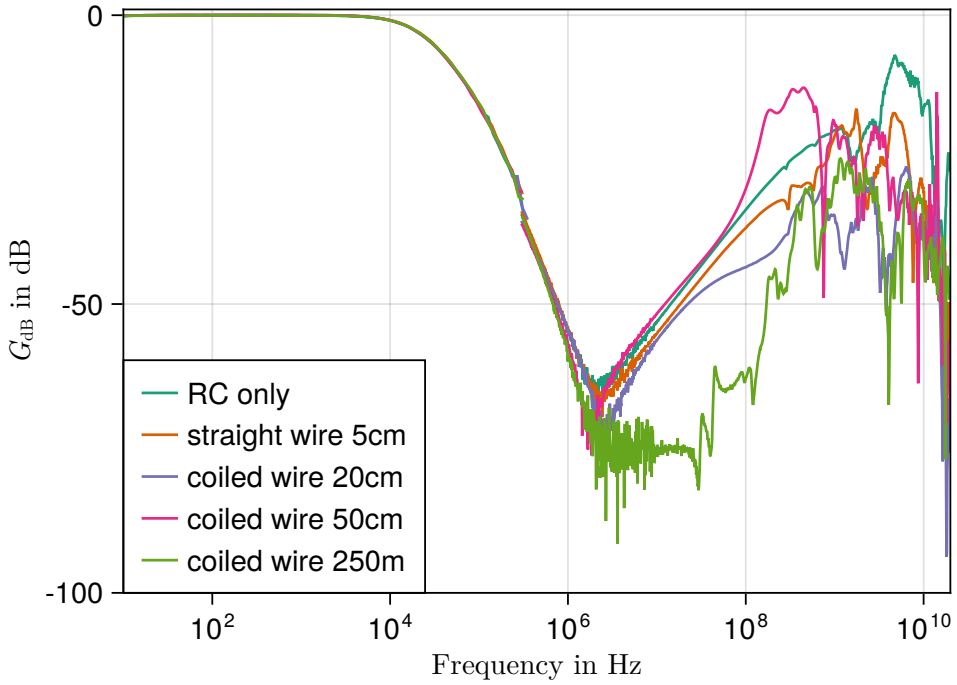

Figure 29: Bode plot comparing multiple test filters. The PCB only (dark green) is being compared to filters with PCB and copper powder stage with various wire lengths, from 5cm to up to 250cm.

The final filter was designed as shown in figure 28 with a wire length of 3 m. The wire has windings with a diameter of 3 mm and is separated into three distinct coils to circumvent parts of the signal that have already been filtered being influenced by the signals at the start of the copper powder stage. A picture of the final filter can be seen in figure 30. Its

frequency response at room temperature is shown in figure 31.

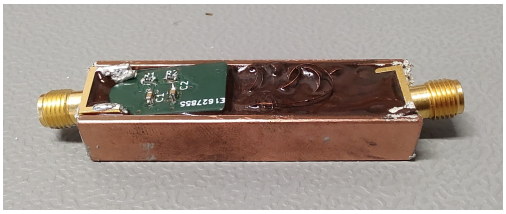

Figure 30: Picture of final filter including the RC filter on a PCB as well as the copper powder filter stage

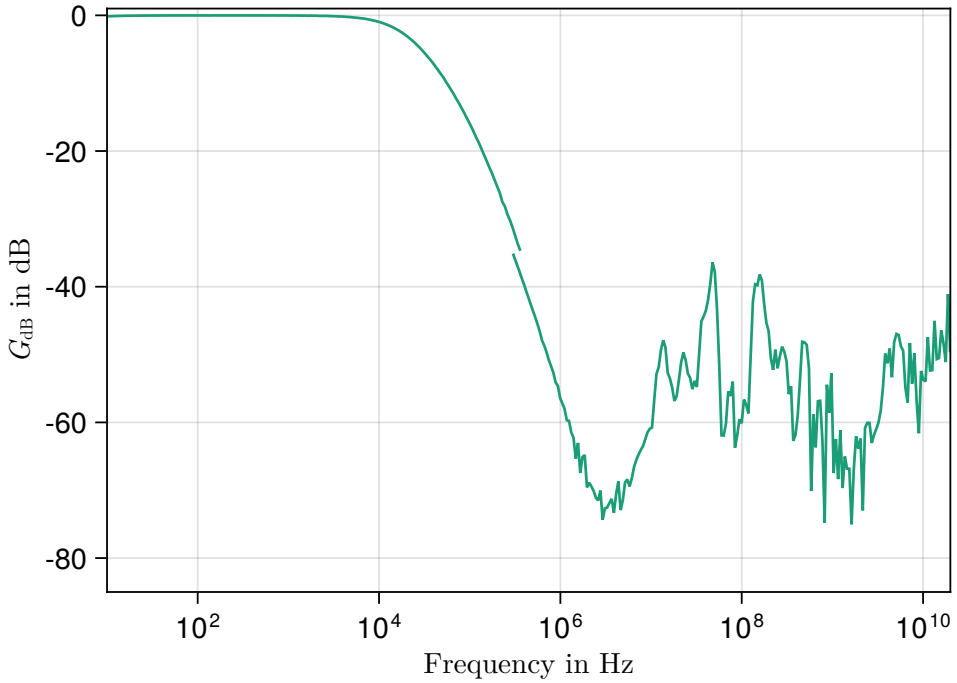

Figure 31: Frequency response of the final filter including both an RC filter stage and a copper powder stage. The filter is shown in figure 30.

Figure 31 shows the frequency response of a filter including both an RC filter stage and a copper powder filter stage. It reaches its lowest transmission point of around $-70\,\mathrm{dB}$ between $10^6\,\mathrm{Hz}$ and $10^7\,\mathrm{Hz}$. Afterward, it has a small reentrance and rises to about $-50\,\mathrm{dB}$ but stays around that range until frequencies as high as $10^{10}\,\mathrm{Hz}$. Compared to the frequency responses shown in figure 29 this filter has higher and more stable attenuation.

4.2 Low Temperature Frequency Response

Since all of these filters are made for cryostat application it is imperative to test them at temperatures comparable to that of a cryostat. The cryostat these filters were built for is the LD dilution refrigerator measurement system made by the company BlueFors [22]. The base temperature is about 10 mK. It is important to know how the cut-off frequency changes with the temperature change. This is the case because, in addition to the changing functionality of the PCB, the cut-off frequency is also influenced by the change in the sample resistance (see Chapter 2.4.1). Both effects at the same time can lead to a cut-off frequency that is too low for the filter to function properly.

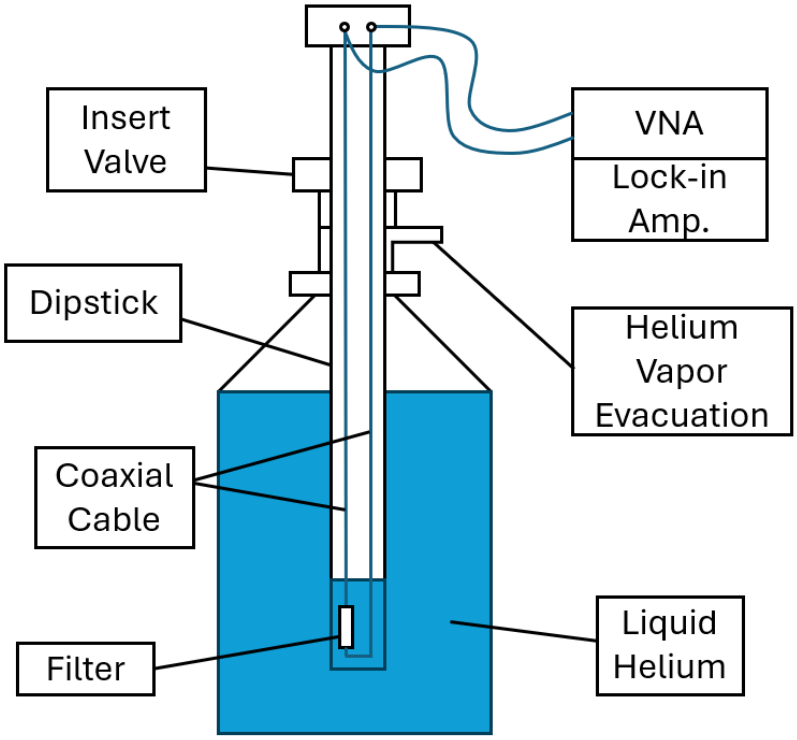

Figure 32: Schematic of a dipstick setup with a helium can. The filter is placed inside the dipstick and then inserted into the helium can. Measurements can be taken via cable that are laid down between the ends of the dipstick.

To test how a change in temperature affects the RC filter stage, as well as the copper filter stage, the filter shown in figure 30 was tested in a dipstick. A device consisting of a pressurized can filled with liquid helium and dipstick, a long metal rod with a coaxial cable

running from the end at RT to the one at 4 K. To test the filter it is connected between two cables on one side of the dipstick. The cable at the other end of the dipstick is then connected to either a VNA or a lock-in amplifier. An airtight valve of the helium can is used as the entrance point for the dipstick. It is now slowly lowered into the liquid helium. The filter can reach a temperature as low as 4 K while its frequency response is measured. The resulting data can be seen in figure 33.

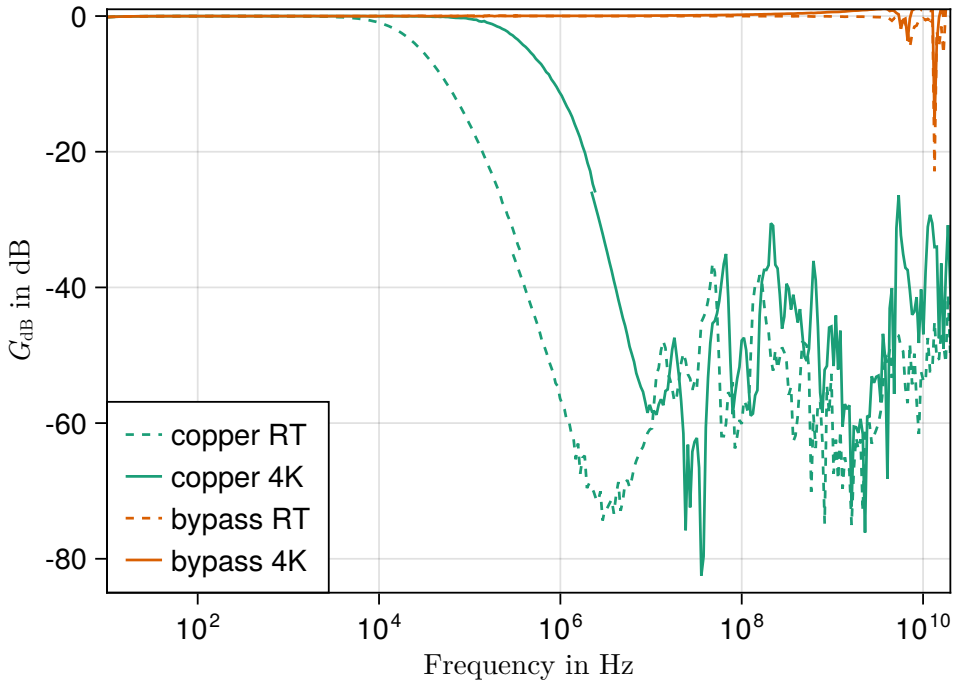

Figure 33: Frequency response of the filter shown in figure 30 at base temperature (4K) compared to its frequency response at room temperature (RT). The figure also includes the transfer of the wires without the filter, called the bypass measurement.

The bypass measurement (only wiring) is included in the calibration of the VNA and should therefore show no loss in transfer. As seen in figure 33 this is the case until about 10^{10} Hz, where the accuracy of the measurement starts to break down. There are only small changes between the bypass measurement at 4 K and RT. This indicates that the calibration of the VNA does not change with temperature and therefore the change in cut-off frequency at low temperature can not be explained by the influence of the cable. The cut-off frequency of the RC filter stage shifts between around 10^4 Hz at room temperature to around 10^5 Hz at 4 K. With that, the slope also shifts back by the same amount. Since the reentrance

does not change its frequency the filter does not reach the same maximal attenuation as at room temperature but starts to increase in transfer again at $10^7\,\mathrm{Hz}$ with a depth of $-60\,\mathrm{dB}$. Referencing equation (18) the shift in cut-off frequency indicates that either the resistance, capacitance, or both of the SMD components decreases at low temperatures. The frequency response of the copper powder stage seems to be relatively comparable between room temperature and the measurement made at $4\,\mathrm{K}$. The transfer still seems to be around $-50\,\mathrm{dB}$ between $10^6\,\mathrm{Hz}$ and $10^{10}\,\mathrm{Hz}$ with a few more outliers reaching up to $-80\,\mathrm{dB}$ and $-30\,\mathrm{dB}$ compared to the frequency response at room temperature.

5 Conclusion and Outlook

Within the scope of this bachelor thesis, a filtering system consisting of an RC filter stage and a copper powder stage was designed, constructed, and investigated.

In Chapter 2 a second-order filter with a cut-off frequency of about 10^4 Hz and a roll-off slope of -20 dB/decade was designed. The influence of a loading resistance on the cut-off frequency and the influence of a coaxial cable on the circuit was illustrated. A PCB was designed to be compatible with SMA connectors and to be included inside a copper box with the copper powder stage. Different factors that start to appear at high frequencies change the function of the RC circuit and lead to a phenomenon known as the reentrance of a filter. This reentrance was modeled with an equivalent circuit to give a guideline on how a circuit could respond with rising frequency.

In Chapter 3 the copper powder stage was designed and optimized. Different tests on the frequency response of different powders and lengths of the wire were made. It was concluded that the optimal choice to maximize attenuation and reduce resonance and stray capacitance was to use a wire length of 3 m in a coiled pattern with a diameter of 3 mm. The wire is then separated into three distinct coils to further reduce transmission between different parts of the wire. The influence of the size of the copper powder was deemed to be negligible. In the last part of the chapter, the stray capacitance between SMA connectors in copper powder was discussed, setting limitations of attenuation for the current filter design.

In Chapter 4 both filter stages were combined into a filtering matrix and tested at room temperature and 4 K with the use of a dipstick. At room temperature, the filter system has a maximum attenuation of -70 dB at 10^6 Hz and a steady attenuation below -40 dB at higher frequencies. At 4 K the cut-off frequency changes to 10^5 Hz but the high-frequency response stays the same. The filter is not as good as commercially available filters that can reach an attenuation of up to -90 dB [31]. Still, since decibel is a logarithmic scale an attenuation -70 dB and a steady frequency response at higher frequencies is applicable in noise measurements.

The optimization of a filter system is a challenging topic since a lot of components have large

influences at high frequencies. Different small optimizations could be easily realized in the future without changing the current design of the filter. One example would be the cascading of resistance and capacitances in the RC stage to reduce the influence of loading resistances. Other optimizations would take a complete redesign of the filter to achieve. A popular way of streamlining the construction of metal powder filters is replacing the wire through a PCB with printed tracks that take on the same role. This also allows for a printed ground line that further increases the functionality of the filter [32]. A good implementation can lead to stable attenuations of around $-80\,\mathrm{dB}$. Another design method used in the commercial construction of metal powder filters is replacing the copper powder epoxy mixture with a silver epoxy paste. this can have an attenuation of up to $-90\,\mathrm{dB}$. Multiple attempts were made during the duration of this bachelor thesis to design such a filter. Since the silver epoxy mixture is highly conductive small damages in the insulation of the wire quickly lead to the shortening of the entire circuit making such a construction challenging. However further investment into this design could lead to working filters with better attenuation than the current design.

References

[1] Cui-Zu Chang et al. "Experimental Observation of the Quantum Anomalous Hall Effect in a Magnetic Topological Insulator". In: *Science* 340.6129 (Apr. 2013), pp. 167–170. DOI: 10.1126/science.1234414. arXiv: 1605.08829 [cond-mat.mes-hall].

[2] Gertjan Lippertz. *The Quantum Anomalous Hall Effect in Magnetically Doped Topological Insulators: A Study of the Current-Induced Breakdown*. 2023.

[3] Frank Pobell. *Matter and Methodes at Low Temperatures*. Springer Berlin, Heidelberg, 2007. ISBN: 978-3-540-46356-6.

[4] Winfield Hill Paul Horowitz. "Learning the Art of Electronics". In: Cambridge University Press, 2015. ISBN: 978-0-52-80926-9.

[5] Kensuke Kobayashi and Masayuki Hashisaka. *Shot Noise in Mesoscopic Systems: From Single Particles to Quantum Liquids*. 2021. DOI: https://doi.org/10.7566/JPSJ.90.102001.

[6] Eva-Maria Liebhaber. "Superconducting Point Contacts on the Topological Insulator Mercury Telluride". MA thesis. Bayerische Julius-Maximilians-Universität Würzburg, 2016.

[7] *DEWEsoft Datenerfassung*. (Accesed: 30.8.2024). URL: https://dewesoft.com/de/blog/was-ist-datenerfassung.

[8] Bryan H. Suits. "Electronics for Physicists: An Introduction". In: Cham: Springer International Publishing, 2023. ISBN: 978-3-031-36364-1. URL: https://doi.org/10.1007/978-3-031-36364-1.

[9] Wolfgang Demtröder. "Experimentalphysik 2 Elektrizität und Optik". In: Springer Spektrum Berlin, Heidelberg, 2018. ISBN: 978-3-662-55790-7. URL: https://doi.org/10.1007/978-3-662-55790-7.

[10] Krishnavedala. *Voltage divider*. (Created: 23.10.2024). URL: https://en.wikipedia.org/wiki/Voltage_divider#/media/File:Resistive_divider2.svg.

[11] *ElectronicsTutorials Passive Low Pass Filter*. (Accesed: 07.08.2024). URL: https://www.electronics-tutorials.ws/filter/filter_2.html.

[12] *Omnicalculator*. (Accesed: 30.8.2024). URL: https://www.omnicalculator.com/physics/cutoff-frequency.

[13] *ADI Analogue Dialogue: Phase Response in Active Filters*. (Accesed: 31.8.2024). URL: https://www.analog.com/en/resources/analog-dialogue/articles/band-pass-response-in-active-filters.html.

[14] *Butterworth Filter Orders*. (Accesed: 30.8.2024). URL: https://en.wikipedia.org/wiki/Low-pass_filter#/media/File:Butterworth_Filter_Orders.svg.

[15] Stanford Research Systems. *About Lock-In Amplifiers*. URL: https://www.thinksrs.com/downloads/pdfs/applicationnotes/AboutLIAs.pdf.

[16] keysight. *Network Analyzer Basics*. URL: https://web.archive.org/web/20200204075722/https://www.keysight.com/upload/cmc_upload/All/BTB_Network_2005-1.pdf.

[17] Analog Devices. *LTspice*. (Accesed: 16.8.2024). URL: https://www.analog.com/en/resources/design-tools-and-calculators/ltspice-simulator.html.

[18] *KICad*. (Accesed: 23.8.2024). URL: https://www.kicad.org/.

[19] *elektronik compendium*. (Accessed: 29.8.2024). URL: https://www.elektronik-kompendium.de/sites/kom/0308051.htm.

[20] Maty Weinberg H. Ward Silver Mark J. Wilson. *The ARRl Handbook for Radio Communications 2010: The Comprehensive Rf Engineering Reference*. Amer Radio Relay League, 2010. ISBN: 0872591468.

[21] *Analog Devices Wiki*. (Accessed: 30.8.2024). URL: https://wiki.analog.com/university/labs/tlines_standing_waves_adalm2000#transmission_lines_general_information.

[22] *BLUEFORS*. (Accessed: 30.8.2024). URL: https://bluefors.com/products.

[23] *reichelt elektronik*. (Accesed: 2.9.2024). URL: https://www.reichelt.de/smd-kerko-0603-47-nf-50v-10-x7r-mlcc-wal-0603b473k500-p346765.html?CCOUNTRY=445&LANGUAGE=de&trstct=pos_0&nbc=1&&r=1.

[24] Ph.D. Jeffrey Cain. *Parasitic Inductance of Multilayer Ceramic Capacitors*. URL: https://kyocera-avx.com/docs/techinfo/CeramicCapacitors/parasitc.pdf.

[25] Marcus O'Sullivan. *Optimize High-Current Sensing Accuracy by Improving Pad Layout of Low-Value Shunt Resistors*. URL: https://www.analog.com/media/en/analog-dialogue/volume-46/number-2/articles/optimize-high-current-sensing-accuracy.pdf.

[26] *Altium PCB Trace Inductance Calculation: How Wide is Too Wide?* (Accessed: 30.8.2024). URL: https://resources.altium.com/p/pcb-trace-inductance-and-width-how-wide-too-wide.

[27] *RAYPCB: How do you calculate the PCB Trace Resistance ?* (Accesed: 9.9.2024). URL: https://www.raypcb.com/trace-resistance-calculator/.

[28] Martin Graham Howard W. Johnson. "High-speed Signal Propagation". In: Prentice Hall PTR, 2003. ISBN: 9780130844088.

[29] John M. Martinis, Michel H. Devoret, and John Clarke. "Experimental tests for the quantum behavior of a macroscopic degree of freedom: The phase difference across a Josephson junction". In: *Phys. Rev. B* 35 (10 Apr. 1987), pp. 4682–4698. DOI: 10.1103/PhysRevB.35.4682. URL: https://link.aps.org/doi/10.1103/PhysRevB.35.4682.

[30] Tildon H. Glisson. *Introduction to Circuit Analysis and Design*. Springer Dordrecht, 2011. ISBN: 978-90-481-9442-1.

[31] Basel Precission Instruments. *Unique Ultra-Stable Low-Noise Electronics Cryogenic Microwave Filter Thermalizers*.

[32] Filipp Mueller; Raymond N. Schouten; Matthias Brauns; Tian Gang; Wee Han Lim; Nai Shyan Lai; Andrew S. Dzurak; Wilfred G. van der Wiel; Floris A. Zwanenburg. *Printed circuit board metal powder filters for low electron temperatures*. DOI: https://doi.org/10.1063/1.4802875.